The Oncologist, 2022, **27**, 389–397
https://doi.org/10.1093/oncolo/oyac034
Advance access publication 28 March 2022
Original Article

Computed Tomography Texture Analysis for Predicting Clinical Outcomes in Patients With Metastatic Renal Cell Carcinoma Treated With Immune Checkpoint Inhibitors

Hyo Jung Park[1], Lei Qin[2,3], Ziad Bakouny[4], Katherine M. Krajewski[2,3], Eliezer M. Van Allen[4], Toni K. Choueiri[4], Atul B. Shinagare[2,3,*]

[1]Department of Radiology and Research Institute of Radiology, University of Ulsan College of Medicine, Asan Medical Center, Seoul, Republic of Korea
[2]Department of Imaging, Dana-Farber Cancer Institute, Harvard Medical School, Boston, MA, USA
[3]Department of Radiology, Brigham and Women's Hospital, Harvard Medical School, Boston, MA, USA
[4]Department of Medical Oncology, Dana-Farber Cancer Institute, Boston, MA, USA

*Corresponding author: Atul B. Shinagare, Department of Radiology, Brigham and Womens Hospital, Harvard Medical School, 75 Francis Street, Boston, MA 02115, USA. Tel.: +1 6176322988; Fax: +1 6175828574; Email: ashinagare@bwh.harvard.edu

Abstract

Background: The treatment responses of immune checkpoint inhibitors in metastatic renal cell carcinoma (mRCC) vary, requiring reliable prognostic biomarkers. We assessed the prognostic ability of computed tomography (CT) texture analysis in patients with mRCC treated with programmed death receptor-1 (PD-1)/programmed death ligand-1 (PD-L1) inhibitors.

Materials and Methods: Sixty-eight patients with mRCC treated with PD-1/PD-L1 inhibitors between 2012 and 2019 were revaluated. Using baseline and first follow-up CT, baseline and follow-up texture models were developed to predict overall survival (OS) and progression-free survival (PFS) using least absolute shrinkage and selection operator Cox-proportional hazards analysis. Patients were divided into high-risk or low-risk group, and the survival difference was assessed using Kaplan-Meier and log-rank test. Multivariable Cox models were constructed by including only the clinical variables (clinical models) and by combining the clinical variables and the texture models (combined clinical-texture models), and their predictive performance was evaluated using Harrell's C-index.

Results: The baseline texture models distinguished longer- and shorter-term survivors for both OS (median, 60.1 vs. 17.0 months; $P = .048$) and PFS (5.2 vs. 2.8 months; $P = .003$). The follow-up texture models distinguished longer- and shorter-term overall survivors (40.3 vs. 15.2 months; $P = .008$) but not for PFS (5.0 vs. 3.6 months; $P = .25$). The combined clinical-texture model outperformed the clinical model in both predicting the OS (C-index, 0.70 vs. 0.63; $P = .03$) and PFS (C-index, 0.63 vs. 0.55; $P = .04$).

Conclusion: CT texture analysis performed at baseline and early after starting PD-1/PD-L1 inhibitors is associated with clinical outcomes of patients with mRCC.

Key words: metastatic renal cell carcinoma; immune checkpoint inhibitors; computed tomography; texture analysis; survival.

Implications for Practice

The diverse treatment outcomes of patients with metastatic renal cell carcinoma (mRCC) following immune checkpoint inhibitor (ICI)-based therapies necessitate reliable prognostic biomarkers. Using computed tomography (CTs) performed at baseline and within 3 months after treatment initiation, the baseline and follow-up texture models were constructed to predict overall survival and progression-free survival. The baseline texture models could distinguish shorter-term and longer-term overall survivors and progression-free survivors, and the follow-up texture models could distinguish shorter-term and longer-term overall survivors. The present study demonstrates that texture analysis using CT obtained before and early after ICI-based treatment may help in predicting treatment outcomes in patients with mRCC.

Introduction

The treatment landscape of metastatic renal cell carcinoma (mRCC) has undergone a radical change in the past 15 years, with agents targeting the mammalian target of rapamycin (mTOR), vascular endothelial growth factor (VEGF), programmed death receptor-1 (PD-1)/programmed death ligand-1 (PD-L1), and cytotoxic T lymphocyte antigen-4 (CTLA-4) axes all becoming part of the standard of care of treatment.[1,2] While these therapies have substantially improved the outcomes of patients with mRCC, the selection of patients for systemic therapies has now become of paramount importance to maximize the efficacy and minimize the toxicity of these therapies for patients.

Multiple studies have investigated biomarkers of response to systemic therapies in mRCC. These biomarkers have been primarily tumor tissue-based and have included infiltrating

Received: 8 August 2021; Accepted: 7 January 2022.

T-cell exhaustion markers,[3] PD-L1 protein expression,[3,4] somatic mutations,[5-7] transcriptomic signatures,[8-10] and histologic features.[11,12] Despite their promise, none of these biomarkers are routinely used in clinical practice for treatment selection, owing to the lack of standardization and their limited predictive ability. Moreover, these methods may be limited by the invasiveness of tissue acquisition and sampling errors related to variations in tissue composition within the tumor.

Tumor heterogeneity is a well-known feature of malignancy that may help predict tumor behavior and outcomes.[13] It can be quantitatively assessed by texture analysis, an imaging processing method used to quantitatively analyze imaging-based spatial composition of lesions that may not be perceptible to the human eye.[14] There is growing evidence that identifying tumor heterogeneity using computed tomography (CT) texture analysis can be helpful in predicting tumor aggressiveness, treatment response, and overall survival (OS) in various cancer subtypes.[15-19]

Prior study from our group in metastatic urothelial cancer showed that CT texture analysis can help predict the durability of response to treatment with immune checkpoint inhibitor (ICI).[20] Given the promising results of CT texture analysis in preceding studies,[15,16,18,19] the potential of CT texture analysis as a prognostic biomarker deserves further exploration. Therefore, the aim of this study was to assess the predictive ability of CT texture analysis for OS and progression-free survival (PFS) in patients with mRCC treated with ICI-based therapies.

Materials and Methods

Study Population

This institutional review board-approved, Health Insurance Portability and Accountability Act-compliant retrospective study was performed at a large cancer referral center. Written informed consent was waived. Inclusion criteria were as follows: (1) patients with mRCC treated at our institute with ICI from January 2012 to February 2019; (2) baseline and first follow-up contrast-enhanced CT of the chest, abdomen, and pelvis available for review; and (3) presence of target lesion(s) per response evaluation criteria in solid tumors (RECIST) 1.1[21] on the baseline CT. Among 129 recruited patients, those without available contrast-enhanced CT(s) at baseline or follow-up (n = 40), and those without any target lesion (n = 21) were excluded. The final cohort consisted of 68 patients (median age, 61 years (interquartile range [IQR], 53-66]; 55 men, 13 women) (Figure 1). The median time interval from baseline CT acquisition to treatment initiation was 17 days (IQR, 10-22 days). The first follow-up CT scan(s) were obtained within 3 months after treatment initiation. Patients' imaging data and clinicopathologic factors including age, sex, histologic type of RCC, and IMDC (International Metastatic RCC Database Consortium) risk category[22,23] were obtained. Patients' medical records were reviewed to record the date of start of treatment, date of disease progression (PD) per RECIST 1.1, and survival data.

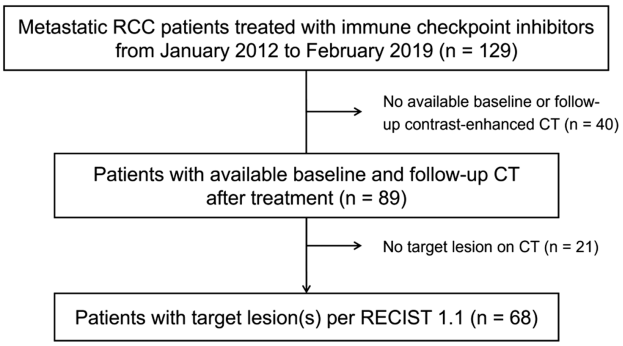

Figure 1. Flow diagram of the patient recruitment process.

Endpoints

The primary endpoints were OS and PFS. OS was defined as the time from treatment initiation and death from any cause, and PFS was defined as the time interval between treatment initiation and tumor progression or death from any cause, whichever occurred first.[24] For both endpoints, patients were censored at last follow-up if an event had not occurred.

CT Acquisition

CT images were acquired on multidetector-row CT scanners with 120 kVP and a tube current maximum of 500 mA with dose modulation. Scans were performed after administration of 75-100 mL nonionic iodine contrast (Ultravist; Bayer HealthCare, Leverkusen, Germany) based on estimated glomerular filtration rate, and empirically timed with chest images obtained in the arterial phase (25-35 seconds delay) and abdominopelvic images obtained in the portal venous phase (60-90 seconds delay). Scans were reconstructed with an axial section thickness of 5 mm.

Tumor Segmentation and Texture Analysis

On CT, among lesions ≥ 1 cm in maximum diameter and lymph nodes ≥ 1.5 cm in short axis, a maximum of two lesions per organ and a total of five lesions per patient were selected as target lesions per RECIST 1.1[21] by a fellowship-trained radiologist with 2 years of experience (H.J.P.) who was blinded to the outcomes. A single slice axial CT image showing maximum size of each lesion was sent to a commercially available texture analysis research software platform (TexRAD Ltd, part of Feedback Plc, Cambridge, UK; www.texrad.org). Using this software, a fellowship-trained radiologist with 2 years of experience (H.J.P.) created the region-of-interest (ROI) of by contouring each lesion under the supervision of another board-certified abdominal radiologist with 10 years of experience (A.B.S.). The texture analysis technique used in this study uses a histogram-based technique[25] which evaluates the gray-level frequency distribution from the pixel intensity in ROIs, retrieving a set of quantifiable texture features: mean (the average value of pixel intensities within the ROI), standard deviation (SD; the variation or dispersion from the mean value), entropy (the complexity of pixel intensities), skewness (the asymmetry of the distribution of the pixel intensity values on the histogram), and kurtosis (a measure of the peakedness of the distribution of the pixel intensity values on the histogram).[14] A total of 10 texture features (five from the baseline CT and five from the follow-up CT) were extracted per lesion. Each texture feature was calculated separately for each target lesion and then averaged for each patient.

Texture Model Development

To investigate the prognostic value of the extracted texture features, we developed texture models using the baseline CT

to predict survival of the patients (baseline texture models) and follow-up CT (follow-up texture models) separately for predicting OS and PFS. For feature selection and model construction, we used the least absolute shrinkage and selection operator (Lasso)-Cox proportional hazards analysis.[26] Considering the small sample size, we implemented leave-one-out cross-validation resampling method[27,28] to validate the performance of the texture models to predict survival of the patients, a method used and validated in prior literature.[29-31] Patient data (n = 68) were divided into two parts, a training set made up of 67 patients and a single patient left for validation. This leave-one-out procedure was repeated a total of 68 times through the whole patient dataset until each patient data was used as the test set, and the test results were aggregated. Lasso-Cox models were built using only the training set to select the regularization parameters, which resulted in feature selection and computation of survival indices on the training sets. Using the median survival index calculated from the training set in the Lasso-Cox model as threshold, patients were categorized into either high-risk or low-risk group. Since the test data was not used in model training process, the test error is an unbiased estimate of the model performance.

Statistical Analysis

Paired t-test was used to compare the value of each texture parameter on baseline and follow-up CT. Kaplan-Meier and log-rank test were used to assess the survival difference between the high-risk and low-risk groups. To predict OS and PFS, clinical models (including age, sex, histologic type of RCC [ie, sarcomatoid/rhabdoid differentiation or not], and the IMDC risk category[32]) and the combined clinical-texture models (including both the clinical variables and the texture models) were constructed by multivariable Cox proportional hazard analysis to predict OS and PFS. We used an automated variable selection method by using the backward elimination with the Akaike information criteria (AIC) as a feature selection rule.[33] The hazard ratio (HR) and 95% confidence intervals (CI) of each variable were calculated. The discriminatory capabilities of the models were evaluated using the AIC and the Harrell's C-index,[34] and the C-indexes were compared using the nonparametric approach described by Kang et al.[35] The calibration capabilities of the models were assessed using a calibration plot[36] that compared the predicted versus the observed probabilities of 2-year OS and 6-month PFS. A two-sided P value < .05 was considered significant. Statistical analysis was done with R (R Foundation for Statistical Computing, Vienna, Austria, http://www.R-project.org, version 4.1.1). Lasso-Cox models were built using "glmnet" package.

Results

Patient Characteristics

The clinical characteristics of the included patients are shown in Table 1. The most common histological subtype of RCC was clear cell RCC (67.6%, 46/68). Sarcomatoid or rhabdoid differentiation was present in 19 patients (27.9%). IMDC risk group categorization was as follows: 9 (13.2%) favorable, 39 (57.4%) intermediate, and 20 (29.4%) poor risk. Patients had a median of two lines of prior systemic therapy for metastatic disease (range, 0-3). ICI-based therapies were the first line of treatment for 32 patients (47.1%). Treatment discontinuation occurred in 61 patients (89.7%) due to PD (80.3%, 49/61) and drug toxicity (16.4%, 10/61). The median treatment

Table 1. Patient characteristics.

Characteristics	Number (%)
Number of patients	68
Age[a]	61 (53-66)
Sex	
Male	55 (80.9)
Female	13 (19.1)
RCC subtype	
Clear cell	46 (67.6)
Papillary	9 (13.2)
Chromophobe	5 (7.4)
Others[b]	8 (11.8)
Sarcomatoid or rhaboid differentiation	
Present	19 (27.9)
Absent	49 (72.1)
IMDC risk category	
Favorable	9 (13.2)
Intermediate	39 (57.4)
Poor	20 (29.4)
Number of prior systemic treatment	
0	32 (47.1)
1	19 (27.9)
≥2	17 (25.0)
Best overall response	
CR or PR	17 (25.0)
SD	19 (27.9)
PD	27 (39.7)
Unknown	5 (7.4)
Treatment regimen[c]	
ICI and VEGF	31 (45.6)
ICI monotherapy	28 (41.2)
ICI combination therapy	6 (8.8)
ICI and clinical trial drugs	3 (4.4)
Reason for off therapy	61 (89.7)
PD	49 (80.3)
Toxicity	10 (16.4)
Consent withdrawal	2 (3.3)
Treatment period (months)[a]	4.6 (1.9-10.2)
Follow-up data[a]	
Follow-up duration (months)	17.0 (9.2-32.2)
OS (months)	21.5 (10.5-32.5)
PFS (months)	5.2 (2.0-8.4)

[a]Data are medians, with first and third quartiles in parentheses.
[b]Xp11.2 translocation type with TFE3 gene fusion (n = 3), collecting duct type (n = 2), fumarate hydratase-deficient type (n = 2), and unclassified type (n = 1).
[c]ICI monotherapy included nivolumab (n = 28) and atezolizumab (n = 1); ICI combination therapy included nivolumab and ipilimumab (n = 5) and durvalumab and tremelimumab (n = 1); ICI and VEGF included atezolizumab and bevacizumab (n = 17), avelumab and axitinib (n = 10), pembrolizumab and axitinib (n = 2), pembrolizumab and lenvatinib (n = 1), and nivolumab and axitinib (n = 1).
Abbreviations: CR, complete response; ICI, immune checkpoint inhibitor; IMDC, International Metastatic RCC Database Consortium; PD, progressive disease; PR, partial response; RCC, renal cell carcinoma; SD, stable disease; VEGF, vascular endothelial growth factor.

period with ICI was 4.6 months (IQR, 1.9-10.2 months). During the follow-up from start of treatment (median, 17.0 months; IQR, 9.2-32.2 months), 54 patients (79.4%) experienced progression, and 40 patients (58.8%) died. The median OS and PFS were 21.5 months (95% CI, 10.5-32.5 months), and 5.2 months (2.0-8.4 months), respectively.

CT Texture Analysis and Development of Outcome Prediction Models

A total of 298 lesions from 68 patients were analyzed. There were 97 lymph nodes (32.6%), 51 lung lesions (17.1%), 41 liver lesions (13.8%), 40 peritoneal nodules (13.4%), 22 adrenal lesions (7.4%), 17 renal lesions (5.7%), 11 pancreatic lesions (3.7%), 10 intramuscular lesions (3.4%), and 9 pleural nodules (3.0%). Details of texture analysis are shown in Table 2.

Using the texture features and patients' outcome data, four Lasso-Cox proportional hazard models were developed: baseline texture model for predicting OS, follow-up texture model for predicting OS, baseline texture model for predicting PFS, and follow-up texture model for predicting PFS. The frequencies of each texture feature to be selected in models are shown in Figure 2. The top features selected in both models for predicting OS were entropy and skewness, and those selected in both models for predicting PFS were entropy and kurtosis.

Performance of CT Texture Models for Predicting OS and PFS

Patients were categorized into either high-risk or low-risk group with the median survival index obtained from training datasets as threshold. For OS, both the baseline and follow-up texture models successfully distinguished longer-term and shorter-term survivors in the test set (Figure 3A and B). In the baseline texture model, the median OS was 60.1 months (95% CI, 19.6-not reached) in the low-risk group and 17.0 months (95% CI, 11.9-32.8) in the high-risk group (P = .048), and in the follow-up texture model, the median OS was 40.3 months (95% CI, 21.7-not reached) and 15.2 months (95% CI, 11.1–32.3) in low- and high-risk group, respectively (P = .008). Representative cases are shown in Figure 4.

For PFS, the baseline texture model successfully distinguished shorter from longer PFS patients in the test set, but the follow-up texture model failed to distinguish the shorter-term from longer-term progression-free survivors (Figure 3C and D). In the baseline texture model, the median PFS was 5.2 months (95% CI, 3.6-23.8) in the low-risk group and 2.8 months (95% CI, 1.7-7.6) in the high-risk group (P = .003). In the follow-up texture model, the median PFS was 5.0 months (95% CI, 3.5-11.9) and 3.6 months (95% CI, 2.4-7.6) in low- and high-risk group, respectively (P = .25).

In a subgroup of the 32 patients without prior systemic treatment (ie, treated with ICI as a first-line therapy), the baseline texture models for OS and PFS discriminated longer- and shorter-term survivors (median OS, not reached vs. 16.8 months [95% CI, 2.9-30.7], P = .03; median PFS, 11.7 months [95% CI, 4.5-33.6] vs. 3.8 months [95% CI, 1.4-7.8], P = .004), and the follow-up texture model for OS also distinguished longer- and shorter-term survivors (median OS, 39.7 months vs. 9.8 months [95% CI, 0.1-19.5], P = .002). The follow-up texture model for PFS could not separate longer-term survivors (median PFS, 6.9 months [95% CI, 4.5-17.1]) and shorter-term survivors (median PFS, 3.6 months [95% CI, 1.4-10.4] (P = .53) (Supplementary Figure S1).

Performance of the Clinical Models and the Combined Clinical-Texture Models for Predicting Outcome

The results of the univariable and the multivariable Cox regression analyses are shown in Supplementary Tables S1 and S2, respectively. For OS, univariable analysis showed that both the baseline and follow-up texture models had significant association with OS (HR, 2.05 [95% CI, 1.07-3.94] and 2.65 [95% CI, 1.38-5.11] for baseline and follow-up texture model, respectively). IMDC risk category also showed significant association with OS (HR, 5.64 [95% CI, 1.29-24.64] for poor category, with favorable category being the reference). None of the other clinicopathologic variables showed significant association with OS ($P \geq .09$). For PFS, on univariable analysis, the baseline texture model had significant association with PFS (HR, 1.84 [95% CI, 1.08-3.12]), whereas follow-up texture model did not demonstrate association with PFS (HR, 1.30 [95% CI, 0.77-2.19]). IMDC risk category was not associated with PFS (HR, 2.12 [95% CI, 0.89-5.07] and 2.42 [95% CI, 0.96-9.08] for intermediate category and poor category,

Table 2. Value of each texture parameter of baseline and follow-up CT.

Parameters	High-risk group, OS	Low-risk group, OS	*P*	High-risk group, PFS	Low-risk group, PFS	*P*
Baseline						
Mean	57.4 ± 19.8	80.5 ± 21.0	<.001	59.5 ± 21.4	74.9 ± 22.7	.01
SD	23.4 ± 7.2	21.1 ± 8.0	.13	23.7 ± 7.4	21.2 ± 7.7	.12
Entropy	4.3 ± 0.2	4.1 ± 0.2	.008	4.3 ± 0.2	4.2 ± 0.2	.007
Skewness	−0.1 ± 0.3	−0.5 ± 0.5	<.001	0.0 ± 0.2	−0.5 ± 0.5	<.001
Kurtosis	0.2 ± 0.7	1.5 ± 1.1	<.001	0.0 ± 0.4	1.5 ± 1.0	<.001
Follow-up						
Mean	66.9 ± 23.9	55.0 ± 14.9	.02	70.1 ± 22.5	51.6 ± 13.5	<.001
SD	22.1 ± 5.5	18.7 ± 5.3	.01	23.3 ± 5.3	17.4 ± 4.2	<.001
Entropy	4.3 ± 0.2	4.0 ± 0.3	<.001	4.4 ± 0.2	3.9 ± 0.3	<.001
Skewness	−0.1 ± 0.3	−0.4 ± 0.3	<.001	−0.3 ± 0.4	−0.2 ± 0.4	.74
Kurtosis	0.3 ± 0.6	1.0 ± 0.7	<.001	0.6 ± 0.7	0.7 ± 0.7	.42

Data are mean ± SD.
Abbreviations: CT, computed tomography; SD, standard deviation.

respectively, with favorable category being the reference). No other clinicopathologic variable (such as age, sex, or histologic subtype of RCC) was associated with PFS ($P \geq .06$).

The clinical model for OS included only the IMDC risk category, which predicted OS with a C-index of 0.63 (95% CI, 0.55-0.71). The combined clinical-texture model for OS was constructed with the follow-up texture model and IMDC risk category, and showed the C-index of 0.70 (95% CI, 0.63-0.78), which was significantly higher than that of the clinical model ($P = .03$). The clinical model for PFS included histology only, and predicted PFS with a C-index of 0.55 (95% CI, 0.50-0.61). The combined clinical-texture model for PFS included the baseline texture model, histology, and age, and showed significantly higher C-index (0.63; 95% CI, 0.51-0.73) for predicting PFS than that of the clinical model ($P = .04$). Calibration plots demonstrated a good correlation between the predicted and observed probability of OS and PFS (Supplementary Figure S2).

Discussion

Our study demonstrated that CT texture analysis performed before and early during treatment with ICI-based therapies can help predict OS and PFS in patients with mRCC. The Lasso-Cox prediction texture models built from baseline CT scans could distinguish shorter-term and longer-term survivors in terms of both OS and PFS, and the follow-up texture models built from CT scans within 3 months after treatment initiation could predict shorter-term and longer-term overall survivors. The combined clinical-texture models outperformed the clinical model for both predicting OS and PFS.

The diverse clinical outcomes of patients with mRCC following ICI-based therapies[37-43] necessitates development of reliable biomarkers to predict treatment outcome and to establish stratified approach in treatment planning for individual patients. Despite the need for reliable prognostic/predictive biomarkers, identifying biomarkers for cancer immunotherapy is challenging because immunity is dynamic and adaptive, and molecular heterogeneity exists in the tumor itself and its microenvironment. We tried to address this unmet need for biomarkers to predict treatment response to ICI, and our results demonstrate that baseline CT texture analysis prior to systemic therapy may be a noninvasive prognostic biomarker for clinical outcomes.

Recently, the use of computer-assisted analyses has increased for various imaging-based diagnostic and predictive tasks, expanding the role of imaging beyond the domain of traditional visual imaging analysis. Not only texture analysis, more advanced techniques such as radiomics and deep learning have also gained attention. However, radiomics and deep learning are highly labor-intensive, time consuming, and owing to their high-dimensionality, are easily challenged by issues of overfitting and reproducibility.[44] Also, due to the complexity of radiomics features and nontransparency of deep learning neural network, their results are usually not intuitive.[45] We developed image-based predictive models using the five distinct histogram-based texture features, which were readily extracted using a commercially available software. In histogram-based texture analysis, the workflow of feature extraction and model development is simple and reproducible, and the results are intuitive as the characteristic of each feature is understandable.

In this study, we used Lasso as a method to select features for texture model development. Feature selection, the

Table 3. Performance of the clinical model and the combined clinical-texture model for predicting OS and PFS.

Outcomes	Clinical model	Combined clinical-texture model	*P*[a]
OS			
AIC	286.4	278.5	
C-index (95% CI)	0.63 (0.52-0.71)	0.70 (0.63-0.78)	.03
PFS			
AIC	416.7	409.8	
C-index (95% CI)	0.55 (0.50-0.61)	0.63 (0.51-0.73)	.04

[a]From comparing C-indexes of the clinical model and the combined clinical-texture model.
Abbreviations: AIC, Akaike information criteria; CI, confidence interval; OS, overall survival; PFS, progression-free survival.

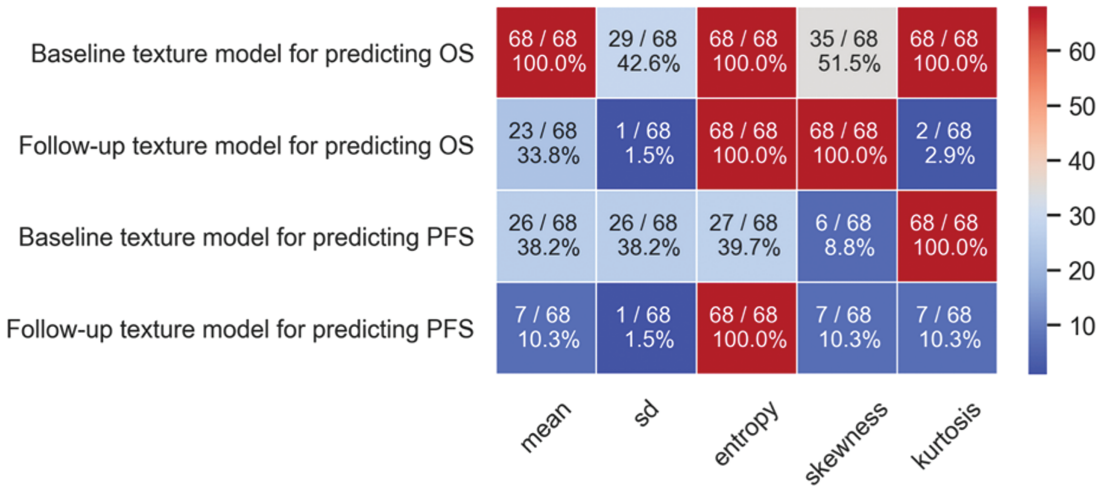

Figure 2. Heatmap showing the selection frequency of each texture feature for predicting OS and PFS. Data in each cell is the number of each texture feature to be selected divided by a total of number of training models with percentages. OS, overall survival; PFS, progression-free survival; SD, standard deviation.

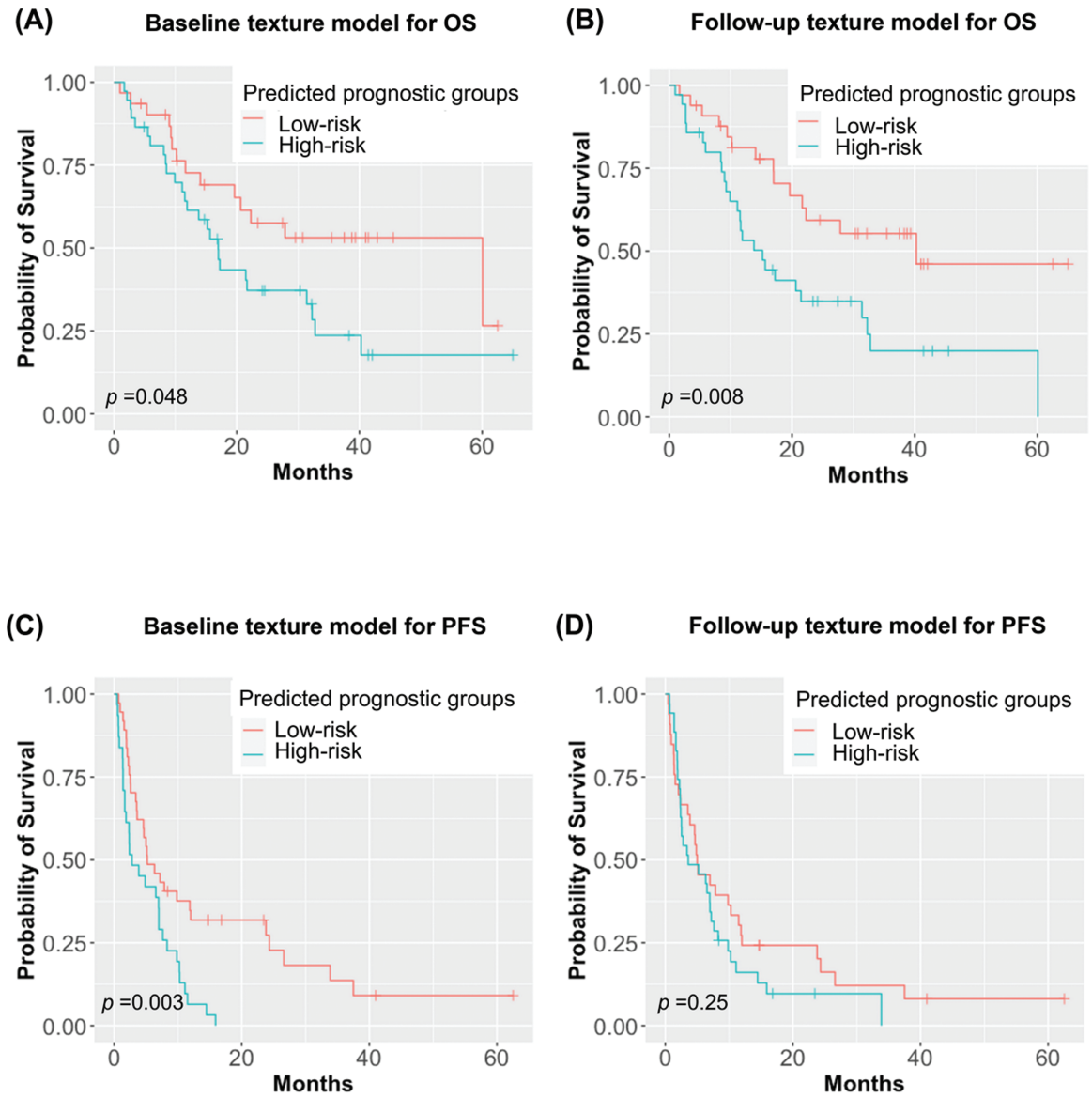

Figure 3. Kaplan-Meier curves of patients stratified by the OS and PFS predicted by texture models. For OS (**A**, **B**), significant differences in patients' survival outcomes were noted between the low-and high-risk groups stratified by texture models in the baseline texture model (**A**) (median OS, 60.1 months vs. 17.0 months; $P = .048$) and follow-up texture model (**B**) (median OS, 40.3 months vs. 15.2 months; $P = .008$). For PFS (**C**, **D**), significant difference was noted in survival outcomes between the low- and high-risk groups in the baseline texture model (**C**, median PFS, 5.2 months vs. 2.8 months; $P = .003$), but not in the follow-up texture model (**D**, median PFS, 5.0 months vs. 3.6 months; $P = .25$). OS, overall survival; PFS, progression-free survival.

process of finding and selecting the most useful features in a data, is a crucial step of the model development process to minimize overfitting. There are several feature selection methods that use regularization technique, such as Lasso, ridge, and elastic net.[46-48] Lasso selects features by penalizing the coefficients of "not-so-significant" features to become zero. Ridge, on the other hand, penalizes the features by reducing their coefficients equally but not to zero. Elastic net uses both the Ridge and Lasso penalties. Lasso is effective in reducing the number of features and performs well when a few features are significant, while it is often unstable when the features are highly correlated, and it cannot select more features than the sample size before it saturates.[49] In our study, to exclude redundant features and produce a parsimonious model, we used Lasso.

Heterogeneity of tumor is a well-known feature of malignancy which may help predict tumor behavior and outcomes.[50] On imaging, tumor heterogeneity can be visualized by the coarseness and irregularity resulting from local spatial variations in image brightness, which can be objectively and quantitatively assessed by texture analysis.[14,15,25] In our study, the most commonly selected texture feature discriminative of high-risk and low-risk groups was entropy, which was selected 100% in baseline texture models for predicting OS and PFS, 100% in follow-up texture model for predicting PFS, and 41.2% in baseline texture model for predicting PFS. Entropy is a statistical measure of randomness reflecting the non-uniformity of pixel intensity, and higher entropy represent increased tumor heterogeneity.[14,25] Higher entropy has been reported to be associated with poor prognosis in

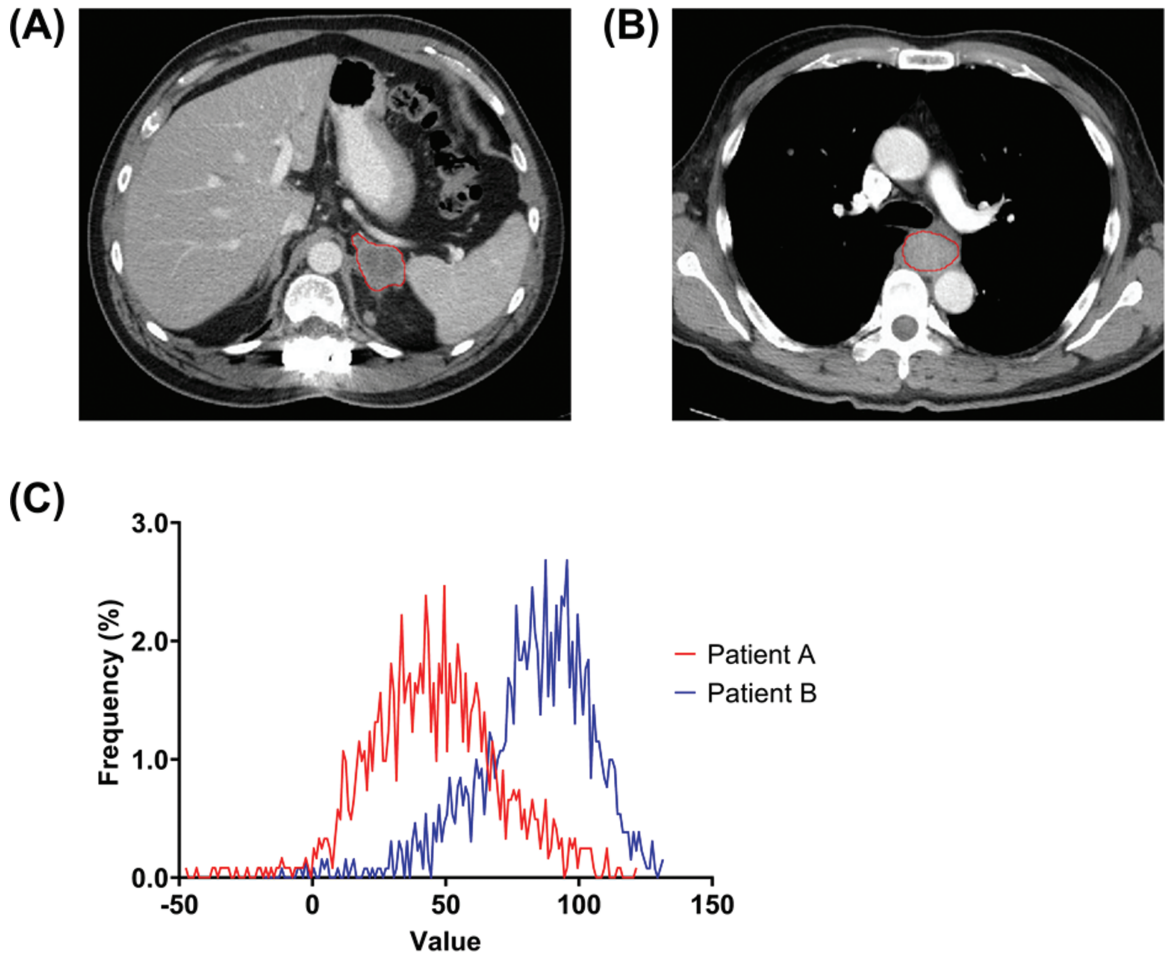

Figure 4. Texture analysis using CT. Contrast-enhanced CT images of the abdomen performed before treatment initiation show (**A**) a metastatic mass in left adrenal gland (red mark) in patient A and (**B**) a metastatic mediastinal lymph node (red mark) in patient B. (**C**) Histogram analysis of the two lesions shows different shapes; higher degree of complexity is noted in patient A's lesion (red line), reflecting higher entropy. Patient A progressed at 2 months and died at 15 months. Patient B survived without progression for more than 40 months. Both the baseline OS texture model and the baseline PFS texture model correctly classified each patient as high-risk and low-risk group, respectively. CT, computed tomography; OS, overall survival; PFS, progression-free survival.

various cancers including lung cancer, urothelial cancer, and RCC,[15,20,51] which is consistent with our result. Kurtosis, a measure of peakedness and tailedness of a probability distribution,[14,25] was the second most commonly selected texture feature. Previous studies also showed that kurtosis is associated with clinical outcome of patients with cancer, again implying tumor heterogeneity evaluated by texture analysis may be predictive of clinical outcome.[15-19] There have been conflicting results on the direction of relationship between kurtosis and prognosis of patients with cancer; several studies showed that lower kurtosis were related with shorter OS,[52,53] as in our study, but others reported higher kurtosis in patients with shorter OS and PFS.[54,55] More studies are needed to further clarify the association between kurtosis and outcome.

Currently, IMDC risk category is the most widely accepted for clinical prognostic stratification in mRCC,[32] which is consistent with our results that the IMDC risk category was the single independent predictor for OS among all clinical variables. When combining the clinical variables and the texture model, both the texture model and IMDC risk category were predictors of OS, and what is more noteworthy is that our baseline texture model was one of the predictors of PFS while IMDC risk category was not. These results indicate that CT texture analysis may have comparative performance to the IMDC risk category, and the potential of CT texture analysis as a useful tool for predicting outcomes in patients with mRCC treated with ICI agents.

Our study has several limitations. First, the retrospective study design may have introduced selection bias. We only included patients who had baseline and first follow-up contrast-enhanced CT. Whether our predictive model is applicable in patients having non-enhanced CT scans is unknown. Second, we only performed the analysis using up to five lesions per patient and up to two lesions per organ, and concerns may arise that this may not represent the characteristics of all targetable lesions. However, this was done according to RECIST 1.1 which also uses the same process for response assessment.[21] Furthermore, the ROI was drawn by a single radiologist; however, high repeatability of texture analysis performed on single ROIs created by single radiologists has been previously demonstrated,[56] and in this way, texture analysis can be easily implemented in clinical practice along with routine response evaluation where a single radiologist interprets the imaging study. Third, due to the small size of the study population, we could not validate our predictive

model in an independent test dataset. We tried to address this by using the "leave-one-out" method which has been previously used.[29-31] Still, our model needs to be further validated with larger, independent cohorts. Despite these limitations, our study indicates that texture analysis has a potential role in predicting outcomes in patients with mRCC treated with immunotherapy as shown in our previous study of patients with metastatic urothelial cancer.

Conclusion

The results of our study suggest that CT texture analysis performed at baseline and early after treatment initiation allows for prediction of OS and PFS in patients with mRCC treated with ICI-based therapies. This may help address the unmet need for a noninvasive prognostic biomarker of treatment response for immunotherapy.

Funding

None declared.

Conflict of Interest

Ziad Bakouny: Genentech/imCORE, Bristol-Myers Squibb (RF), UpToDate (H); **Eliezer M. Van Allen**: Tango Therapeutics, Genome Medical, Invitae, Enara Bio, Janssen, Manifold Bio, Monte Rosa (C/A), Novartis, BMS (RF), Tango Therapeutics, Genome Medical, Syapse, Enara Bio, Manifold Bio, Microsoft, Monte Rosa (OI), Roche/Genentech (travel reimbursement), Institutional patents filed on chromatin mutations and immunotherapy response, and methods for clinical interpretation; intermittent legal consulting on patents for Foaley & Hoag (Patents); **Toni K. Choueiri:** AstraZeneca, Aveo, Bayer, Bristol-Myers Squibb/ER Squibb and Sons LLC, Cerulean,Corvus, Eisai, EMD Serono, Exelixis, Foundation Medicine Inc., Genetech, GlaxoSmithKline, Heron Therapeutics, Infinity Pharma, Ipsen, Jansen Oncology, IQVIA, Lily, Merck, NCCN, NiKang, Novartis, Peloton, Pfizer, Prometheus Labs, Roche, Sanofi/Avantis, Surface Oncology, Pionyr, Tempest (C/A, H), Dana-Farber/Harvard Cancer Center Kidney SPORE (2P50CA101942-16) and Program 5P30CA006516-56, the Kohlberg Chair at Harvard Medical School and the Trust Family, Michael Brigham, and Loker Pinard Funds for Kidney Cancer Research at DFCI (RF); **Atul B. Shinagare:** Virtualscopics and Imaging Endpoints (C/A). The other authors indicated no financial relationships.

(C/A) Consulting/advisory relationship; (RF) Research funding; (E) Employment; (ET) Expert testimony; (H) Honoraria received; (OI) Ownership interests; (IP) Intellectual property rights/inventor/patent holder; (SAB) Scientific advisory board

Author Contributions

Conception/design: A.B.S. Provision of study material or patients: A.B.S. Collection and/or assembly of data: H.J.P. Data analysis and interpretation: H.J.P., L.Q., Z.B., A.B.S. Manuscript writing: H.J.P., L.Q., Z.B., K.M.K., E.M.V.A., T.K.C., A.B.S. Final approval of manuscript: H.J.P., L.Q., Z.B., K.M.K., E.M.V.A., T.K.C., A.B.S.

Data Availability

The data underlying this article will be shared on reasonable request to the corresponding author.

Supplementary Material

Supplementary material is available at *The Oncologist* online.

References

1. National Comprehensive Cancer Network. *NCCN Clinical Practice Guidelines in Oncology: Kidney Cancer*; 2020. Accessed July 31, 2021. https://www.nccn.org/professionals/physician_gls/pdf/kidney.pdf.
2. Choueiri TK, Kaelin WG. Targeting the HIF2–VEGF axis in renal cell carcinoma. *Nat Med*. 2020;26(10):1519-1530.
3. Pignon JC, Jegede O, Shukla SA, et al. irRECIST for the evaluation of candidate biomarkers of response to nivolumab in metastatic clear cell renal cell carcinoma: analysis of a phase ii prospective clinical trial. *Clin Cancer Res*. 2019;25(7):2174-2184.
4. Flaifel A, Xie W, Braun DA, et al. PD-L1 expression and clinical outcomes to cabozantinib, everolimus, and sunitinib in patients with metastatic renal cell carcinoma: analysis of the randomized clinical trials METEOR and CABOSUN. *Clin Cancer Res*. 2019;25(20):6080-6088.
5. Miao D, Margolis CA, Gao W, et al. Genomic correlates of response to immune checkpoint therapies in clear cell renal cell carcinoma. *Science*. 2018:359(6377):801-806.
6. Braun DA, Ishii Y, Walsh AM, et al. Clinical validation of PBRM1 alterations as a marker of immune checkpoint inhibitor response in renal cell carcinoma. *JAMA Oncol*. 2019;5(11):1631-1633.
7. Braun DA, Hou Y, Bakouny Z, et al. Interplay of somatic alterations and immune infiltration modulates response to PD-1 blockade in advanced clear cell renal cell carcinoma. *Nat Med*. 2020;26(6):909-918.
8. Motzer RJ, Robbins PB, Powles T, et al. Avelumab plus axitinib versus sunitinib in advanced renal cell carcinoma: biomarker analysis of the phase 3 JAVELIN Renal 101 trial. *Nat Med*. 2020;26(11):1733-1741.
9. McDermott DF, Huseni MA, Atkins MB, et al. Clinical activity and molecular correlates of response to atezolizumab alone or in combination with bevacizumab versus sunitinib in renal cell carcinoma. *Nat Med*. 2018;24(6):749-757.
10. Motzer RJ, Banchereau R, Hamidi H, et al. Molecular subsets in renal cancer determine outcome to checkpoint and angiogenesis blockade. *Cancer Cell*. 2020;38(6):803-817.e804.
11. Bakouny Z, Braun DA, Shukla SA, et al. Integrative molecular characterization of sarcomatoid and rhabdoid renal cell carcinoma. *Nat Commun*. 2021;1(1):808.
12. Tannir NM, Signoretti S, Choueiri TK, et al. Efficacy and safety of nivolumab plus ipilimumab versus sunitinib in first-line treatment of patients with advanced sarcomatoid renal cell carcinoma. *Clin Cancer Res*. 2021;27(1):78-86.
13. Shipitsin M, Campbell LL, Argani P, et al. Molecular definition of breast tumor heterogeneity. *Cancer Cell*. 2007;11(3):259-273.
14. Lubner MG, Smith AD, Sandrasegaran K, et al. CT texture analysis: definitions, applications, biologic correlates, and challenges. *Radiographics*. 2017;37(5):1483-1503.
15. Goh V, Ganeshan B, Nathan P, et al. Assessment of response to tyrosine kinase inhibitors in metastatic renal cell cancer: CT texture as a predictive biomarker. *Radiology*. 2011;261(1):165-171.
16. O'Connor JP, Rose CJ, Waterton JC, et al. Imaging intratumor heterogeneity: role in therapy response, resistance, and clinical outcome. *Clin Cancer Res*. 2015;21(2):249-257.
17. Sasaguri K, Takahashi N. CT and MR imaging for solid renal mass characterization. *Eur J Radiol*. 2018;99(1):40-54.
18. Ladwa R, Roberts KE, O'Byrne KJ, et al. Quantitative CT texture assessment of tumour heterogeneity to predict those

patients with non-small cell lung cancer most likely to benefit from immune checkpoint inhibitors. *J Clin Oncol*. 2018;36(15):e21027-e21027.
19. Durot C, Mule S, Soyer P, et al. Metastatic melanoma: pretreatment contrast-enhanced CT texture parameters as predictive biomarkers of survival in patients treated with pembrolizumab. *Eur Radiol*. 2019;29(6):3183-3191.
20. Alessandrino F, Gujrathi R, Nassar AH, et al. Predictive role of computed tomography texture analysis in patients with metastatic urothelial cancer treated with programmed death-1 and programmed death-ligand 1 inhibitors. *Eur Urol Oncol*. 2020;3(5):680-686.
21. Eisenhauer EA, Therasse P, Bogaerts J, et al. New response evaluation criteria in solid tumours: revised RECIST guideline (version 1.1). *Eur J Cancer*. 2009;45(2):228-247.
22. Heng DY, Xie W, Regan MM, et al. Prognostic factors for overall survival in patients with metastatic renal cell carcinoma treated with vascular endothelial growth factor-targeted agents: results from a large, multicenter study. *J Clin Oncol*. 2009;27(34):5794-5799.
23. Heng DY, Xie W, Regan MM, et al. External validation and comparison with other models of the International Metastatic Renal-Cell Carcinoma Database Consortium prognostic model: a population-based study. *Lancet Oncol*. 2013;14(2):141-148.
24. U.S. Food and Drug Administration. *Clinical Trial Endpoints for the Approval of Cancer Drugs and Biologics*. Accessed July 31, 2021. https://www.fda.gov/regulatory-information/search-fda-guidance-documents/clinical-trial-endpoints-approval-cancer-drugs-and-biologics.
25. Ganeshan B, Miles KA. Quantifying tumour heterogeneity with CT. *Cancer Imaging*. 2013;13(1):140-149.
26. Simon N, Friedman J, Hastie T, et al. Regularization paths for cox's proportional hazards model via coordinate descent. *J Stat Softw*. 2011;39(5):1-13.
27. Gelfand AE. Model determination using sampling-based methods. In: Gilks WR, Richardson S, Spiegelhalter DJ eds. *Markov Chain Monte Carlo in Practice*. CRC Press; 1996:145-161.
28. Efron B. Estimating the error rate of a prediction rule—improvement on cross-validation. *J Am Stat Assoc*. 1983;78(382):316-331.
29. Yu KH, Zhang C, Berry GJ, et al. Predicting non-small cell lung cancer prognosis by fully automated microscopic pathology image features. *Nat Commun*. 2016;7(1):12474. https://doi.org/10.1038/ncomms12474.
30. O'Connell PJ, Zhang WJ, Menon MC, et al. Biopsy transcriptome expression profiling to identify kidney transplants at risk of chronic injury: a multicentre, prospective study. *Lancet*. 2016;388(10048):983-993.
31. Michiels S, Le Maitre A, Buyse M, et al. Surrogate endpoints for overall survival in locally advanced head and neck cancer: meta-analyses of individual patient data. *Lancet Oncol*. 2009;10(4):341-350.
32. Ko JJ, Xie W, Kroeger N, et al. The International Metastatic Renal Cell Carcinoma Database Consortium model as a prognostic tool in patients with metastatic renal cell carcinoma previously treated with first-line targeted therapy: a population-based study. *Lancet Oncol*. 2015;16(3):293-300.
33. Moons KG, Altman DG, Reitsma JB, et al. Transparent reporting of a multivariable prediction model for individual prognosis or diagnosis (TRIPOD): explanation and elaboration. *Ann Intern Med*. 2015;162(1):W1-73.
34. Harrell FE Jr., Lee KL, Mark DB. Multivariable prognostic models: issues in developing models, evaluating assumptions and adequacy, and measuring and reducing errors. *Stat Med*. 1996;15(4):361-387.
35. Kang L, Chen W, Petrick NA, et al. Comparing two correlated C indices with right-censored survival outcome: a one-shot nonparametric approach. *Stat Med*. 2015;34(4):685-703.
36. Crowson CS, Atkinson EJ, Therneau TM. Assessing calibration of prognostic risk scores. *Stat Methods Med Res*. 2016;25(4):1692-1706.
37. Motzer RJ, Escudier B, McDermott DF, et al. Nivolumab versus everolimus in advanced renal-cell carcinoma. *N Engl J Med*. 2015;373(19):1803-1813.
38. Hwang I, Park I, Yoon SK, et al. Hyperprogressive disease in patients with urothelial carcinoma or renal cell carcinoma treated with PD-1/PD-L1 inhibitors. *Clin Genitourin Cancer*. 2020;18(2):e122-e133.
39. Refae S, Gal J, Brest P, et al. Hyperprogression under immune checkpoint inhibitor: a potential role for germinal immunogenetics. *Sci Rep*. 2020;10(1):3565.
40. Motzer RJ, Rini BI, McDermott DF, et al. Nivolumab plus ipilimumab versus sunitinib in first-line treatment for advanced renal cell carcinoma: extended follow-up of efficacy and safety results from a randomised, controlled, phase 3 trial. *Lancet Oncol*. 2019;20(10):1370-1385.
41. Motzer RJ, Penkov K, Haanen J, et al. Avelumab plus axitinib versus sunitinib for advanced renal-cell carcinoma. *N Engl J Med*. 2019;380(12):1103-1115.
42. Rini BI, Plimack ER, Stus V, et al. Pembrolizumab plus axitinib versus sunitinib for advanced renal-cell carcinoma. *N Engl J Med*. 2019;380(12):1116-1127.
43. Choueiri TK, Powles T, Burotto M, et al. Nivolumab plus Cabozantinib versus Sunitinib for advanced renal-cell carcinoma. *N Engl J Med*. 2021;384(9):829-841.
44. Park JE, Park SY, Kim HJ, et al. Reproducibility and generalizability in radiomics modeling: possible strategies in radiologic and statistical perspectives. *Korean J Radiol*. 2019;20(7):1124-1137.
45. Buhrmester V, Münch D, Arens M. Analysis of explainers of black box deep neural networks for computer vision: a survey. arXiv: 1911.12116v1 [cs.AI]. 2019. Accessed June 03, 2021. https://arxiv.org/abs/1911.12116.
46. Zou H, Hastie T. Regularization and variable selection via the elastic net. *J R Statist Soc B*. 2005;67(2):301-320.
47. Ogutu JO, Schulz-Streeck T, Piepho HP. Genomic selection using regularized linear regression models: ridge regression, lasso, elastic net and their extensions. *BMC Proc*. 2012;6(suppl 2):S10.
48. Friedman J, Hastie T, Tibshirani R. Regularization paths for generalized linear models via coordinate descent. *J Stat Softw*. 2010;33(1):1-22.
49. Zou H. The adaptive lasso and its oracle properties. *J Am Stat Assoc*. 2006;101(476):1418-1429.
50. Nelson DA, Tan TT, Rabson AB, et al. Hypoxia and defective apoptosis drive genomic instability and tumorigenesis. *Genes Dev*. 2004;18(17):2095-2107.
51. Ahn SY, Park CM, Park SJ, et al. Prognostic value of computed tomography texture features in non-small cell lung cancers treated with definitive concomitant chemoradiotherapy. *Invest Radiol*. 2015;50(10):719-725.
52. Ng F, Ganeshan B, Kozarski R, et al. Assessment of primary colorectal cancer heterogeneity by using whole-tumor texture analysis: contrast-enhanced CT texture as a biomarker of 5-year survival. *Radiology*. 2013;266(1):177-184.
53. Weiss GJ, Ganeshan B, Miles KA, et al. Noninvasive image texture analysis differentiates K-ras mutation from pan-wildtype NSCLC and is prognostic. *PLoS One*. 2014;9(7):e100244.
54. Sandrasegaran K, Lin Y, Asare-Sawiri M, et al. CT texture analysis of pancreatic cancer. *Eur Radiol*. 2019;29(3):1067-1073.
55. Haider MA, Vosough A, Khalvati F, et al. CT texture analysis: a potential tool for prediction of survival in patients with metastatic clear cell carcinoma treated with sunitinib. *Cancer Imaging*. 2017;17(1):4.
56. Xu F, Ma X, Wang Y, et al. Ct texture analysis can be a potential tool to differentiate gastrointestinal stromal tumors without kit exon 11 mutation. *Eur J Radiol*. 2018;107(1):90-97.